Atmos. Chem. Phys. Discuss., 12, 17151–17185, 2012
www.atmos-chem-phys-discuss.net/12/17151/2012/
doi:10.5194/acpd-12-17151-2012

Atmospheric Chemistry and Physics Discussions

Impact of anthropogenic emission on air-quality over a megacity – revealed from an intensive atmospheric campaign during the Chinese Spring Festival

K. Huang[1,2], G. Zhuang[1], Y. Lin[1], Q. Wang[1], J. S. Fu[2], R. Zhang[1], J. Li[1,3], C. Deng[1], and Q. Fu[3]

[1]Center for Atmospheric Chemistry Study, Department of Environmental Science and Engineering, Fudan University, Shanghai, 200433, China
[2]Department of Civil and Environmental Engineering, The University of Tennessee, Knoxville, TN 37996, USA
[3]Shanghai Environmental Monitoring Center, Shanghai, 200030, China

Received: 28 May 2012 – Accepted: 21 June 2012 – Published: 12 July 2012

Correspondence to: G. Zhuang (gzhuang@fudan.edu.cn) and J. S. Fu (jsfu@utk.edu)

Published by Copernicus Publications on behalf of the European Geosciences Union.

Abstract

The Chinese Spring Festival is one of the most important traditional festivals in China. The peak transport in the Spring Festival season (spring travel rush) provides a unique opportunity for investigating the impact of human activities on air quality in the Chinese megacities as emission sources varied and fluctuated greatly prior to, during and after the festival. Enhanced vehicular emission during the spring travel rush before the festival resulted in high level pollutants of NO_x ($270\,\mu g\,m^{-3}$), CO ($2572\,\mu g\,m^{-3}$), BC ($8.5\,\mu g\,m^{-3}$) and extremely low single scattering albedo of 0.70, indicating strong fresh combustion. Organics contributed most to $PM_{2.5}$, followed by NO_3^-, NH_4^+, and SO_4^{2-}. During the Chinese Lunar New Year's Eve and Day, widespread usage of fireworks burning caused heavy pollution of extremely high aerosol mass concentration, scattering coefficient, SO_2 and NO_x. Due to the spring travel rush after the festival, anthropogenic emission gradually climbed and mirrored corresponding increases in the aerosol components and gaseous pollutants. Secondary inorganic aerosol (SO_4^{2-}, NO_3^-, and NH_4^+) accounted for a dominant fraction of 74 % in $PM_{2.5}$ due to the enhanced human activities, e.g. higher demand of energy usage from returned residents and re-open of factories and construction sites, more vehicle mileages due to returned workers and expanded public transportation. The average visibility during whole study period was less than 6 km. It was estimated that about 50 % of the total light extinction was due to the high water vapor in the atmosphere. Of the aerosol extinction, organic aerosol had the largest contribution of 47 %, followed by sulfate ammonium, nitrate ammonium and EC of 22 %, 14 %, and 12 %, respectively. Our results indicated the dominant role of traffic-related aerosol species (i.e. organic aerosol, nitrate and EC) on the formation of air pollution, and suggested the importance of controlling vehicle numbers and emissions in mega-cities of China as its population and economy continue to grow.

ACPD

12, 17151–17185, 2012

1 Introduction

China is currently playing an important role in the global economic growth and renaissance. The expansion of urban population has resulted in tremendous increases in energy consumption, emissions of air pollutants and bad air quality days in megacities, city clusters, and their immediate vicinities. Air pollution has become one of the top environmental concerns in China. Tropospheric NO_2 column over China has experienced a large growth over Eastern China, especially above the industrial areas with a fast economical growth (van der A et al., 2006). Although PM_{10} index was reported in a decreasing trend (Chan and Yao, 2008), some aerosol components such as black carbon (BC) and organic carbon increased since 2000 based on an anthropogenic emission inventory of China developed for 1990–2005 (Lei et al., 2011). Fossil-fuel combustion is the main source for BC in East Asia (Zhang et al., 2009a). The heating rate from fossil fuel containing BC is about 100 % larger than biomass burning containing BC, and Asia was also subject to large ratio of BC-to-SO_2 emissions, an index for the net warming (Ramana et al., 2010). As many developing countries and regions are becoming more industrialized, emissions of air pollutants are likely to increase dramatically. Hence, there is a great need to implement control measures to improve air quality and protect public health. In China, the Yangtze River Delta, Beijing and the Pearl River Delta are the most economically vibrant regions. SO_2 emission from coal-fired power sector in China was projected to decrease since 2005, attributed mainly to the wide application of the flue gas desulfurization (FGD) technology (Zhao et al., 2008). The surface annual SO_2 concentration was also observed to decrease after 2005 in Shanghai due to the close of dirty and unefficient power plant units and new technology implemented (Y.F. Lin, manuscript in preparation, 2012). Controlling industrial facilities and mobile sources have been testified to be an efficient way to reduce SO_2, NO_x, NMVOC and PM_{10} during the 2008 Beijing Olympic Game (Wang et al., 2010). A model study using the Model-3/CMAQ (Community Multi-scale Air Quality) stated that upgrading to National IV emission standards is an effective way and can reduce daily averaged

ACPD
12, 17151–17185, 2012

NO_2 and PM_{10} concentrations by 11.7 ppbv and 21.3 $\mu g\,m^{-3}$ for the Pearl River Delta region (Che et al., 2011).

Shanghai is China's most populous urban area and has a total residential population of about 23 million. Of which about 9 million people are temporary residents from the other provinces and cities, which accounted for 39 % of Shanghai's total population (SMSB, 2011). In this study, we conducted an intensive field campaign in Shanghai around the 2008 Chinese Spring Festival (Lunar New Year) travel season in 2009, which is also referred as "Chunyun" in Chinese or the "spring travel rush". During this period, extremely high traffic inflows and outflows would happen as numerous migrant residents would go back to their home city to reunite with their families and celebrate the traditional Chinese Spring Festival. The transport system, e.g. trains, airplanes and road buses, would experience tremendous challenge. In 2009, the total journeys during the spring travel rush reached about 23 billion, which exceeded the whole population of China. Most people chose to travel via road traffic, reaching about 21 billion journeys. Thus, the Chinese new year exodus is also regarded as the world's largest annual migration (BBC, 2009). Due to tremendous fluctuations of human activities, the emission sources are expected to vary greatly. Thus, this study provides us a very good opportunity to evaluate the impact of anthropogenic emission (e.g. vehicular and industrial emission) variations on the aerosol chemical composition, optical properties and the atmospheric visibility. Our previous research results found out the traffic restrictions on the world car-free days (22 September) in multi-years over Shanghai almost had no improvement on the air quality. This is due to that the control measures implemented on both time durations and restriction areas were very limited (personal communication). While in this study, the long Spring Festival travel season provided us a natural atmospheric experiment to evaluate these effects. To our best knowledge, there were rare reports on the impact of emission variations on air quality in megacities prior to, during and after the Chinese Spring Festival.

ACPD
12, 17151–17185, 2012

2 Methodology

2.1 Aerosol and trace gases measurement

The Thermo Scientific TEOM 1405-D monitor simultaneously measured $PM_{2.5}$, PM-Coarse ($PM_{10-2.5}$) and PM_{10} mass concentration upon an oscillating balance. Particulate matters accumulating on a filter mounted changes in the frequency of oscillation, which were related to the mass of material accumulating on the filter, were detected in quasi-real-time and converted by a microprocessor into an equivalent PM mass concentration every few seconds, as a 10 min running average. Sampler split a PM_{10} sample stream into its fine ($PM_{2.5}$) and coarse ($PM_{10-2.5}$) fractions using a USEPA-designed virtual impactor for the additional 2.5 µm cutpoint. The total flow rate operated at 16.67 l min^{-1}, and two separate flow controllers maintained the coarse particle stream at 1.67 l min^{-1} and the fine particle stream at 3.0 l min^{-1}. PM concentrations were averaged and used at intervals of 1 h in this study. Trace gases instruments included 43i SO_2 analyzer, 42i NO-NO_2-NO_x analyzer, 49i O_3 analyzer and 48i CO analyzer. The routine QA/QC included the daily zero/standard calibration, span and range check, station environmental control, staff certification, etc., according to the Technical Guideline of Automatic Stations of Ambient Air Quality in Shanghai based on the national specification HJ/T193–2005, which was developed following the technical guidance established by the US Environmental Protection Agency (USEPA, 1998). The multi-point calibrations were applied upon initial installation of the instruments at the routine intervals of every week. And the two-point calibrations were applied on a daily basis.

ACPD
12, 17151–17185, 2012

2.2 Measurement of aerosol optical properties

2.2.1 Aerosol scattering coefficient measurement

A nephelometer (EcoTech, M9003) was used to continuously measure the aerosol scattering coefficient (σ_{sp}) at the wavelength of 520 nm. It has a detection limit of less than 0.3 M m^{-1} with 60 s integration and a light scattering angle of 10–170°. Air was pumped at a flow rate of 5 l min^{-1} into a heating system. The processor-controlled heating system automatically maintained the relative humidity in the chamber below 40 %. Zero calibrations were performed daily with particle-free air to subtract the Rayleigh scattering from the total light scattering coefficient. Span calibrations were performed daily using 99.99 % CO_2.

2.2.2 BC (aerosol absorption coefficient) measurement

An aethalometer (AE-21, Magee Scientific Co.) equipped with a $PM_{2.5}$ inlet impactor was used to continuously measure the concentration of BC at the wavelength of 880 and 370 nm. The aethalometer measures BC concentrations by collecting the particles on a rolled quartz filter with a cellulose fiber backing, and continuously monitoring the transmission intensity of light beams at 880 and 370 nm wavelengths. The theory of calculating BC concentration could be found elsewhere (Magee-Scientific, 2005). To convert the BC mass concentration to the absorption coefficient (σ_{ap}), an attenuation coefficient of 16.6 and 39.5 m^2 g^{-1} was used for 880 and 370 nm, respectively. As the aerosol scattering coefficient was obtained at 520 nm as stated above, we have to convert σ_{ap} at 520 nm from the Angstrom absorption exponent δ_{ap}. $\delta_{ap} = -\mathrm{d}\log(\sigma_{ap})/\mathrm{d}\log(\lambda)$. The δ_{ap} thus obtained was used in the Angstrom relation ($\delta_{ap}(\lambda) = \beta_{ap}\lambda^{-\delta}$) to obtain the absorption coefficient at required wavelength. Then we can obtain the aerosol absorption coefficient and scattering coefficient at the same wavelength of 520 nm. The single scattering albedo (SSA) can be calculated using $\omega = \sigma_{sp}/(\sigma_{ap} + \sigma_{sp})$.

ACPD
12, 17151–17185, 2012

2.3 Manual sampling

Aerosol samples of TSP and $PM_{2.5}$ were collected on Whatman® 41 filters (Whatman Inc., Maidstone, UK) using medium-volume samplers manufactured by Beijing Geological Instrument-Dickel Co., Ltd. (model: TSP/PM_{10}/$PM_{2.5}$-2; flow rate: 77.59 l min^{-1}). Aerosol samples of PM_{10} were collected on Whatman quartz microfiber filters (QM/A, 18.5 cm × 23.7 cm) using the high-volume sampler (Thermo, flow rate: 1.00 m^3 min^{-1}). All the samplers were co-located with the online instruments on the roof (~30 m) of the 4th Teaching Building at Fudan University, Shanghai. The duration time of sampling was generally 24 h. More samples with shorter duration time were collected during the heavy haze days. The filters before and after sampling were weighed using an analytical balance (model: Sartorius 2004MP) with a reading precision 10 mg after stabilizing in constant temperature (20 ± 1 °C) and humidity (40 ± 1 %). All the procedures were strictly quality controlled to avoid the possible contamination of samples.

2.4 Chemical analysis

2.4.1 Ion analysis

One-fourth of each sample and blank filter was extracted ultrasonically by 10 ml deionized water (18 MΩ cm^{-1}). Eleven inorganic ions (SO_4^{2-}, NO_3^-, F^-, Cl^-, NO_2^-, PO_4^{3-}, NH_4^+, Na^+, K^+, Ca^{2+}, Mg^{2+}) and four organic acids (formic, acetic, oxalic, and methylsulfonic acid (MSA)) were analyzed by Ion Chromatography (ICS 3000, Dionex), which consisted of a separation column (Dionex Ionpac AS 11), a guard column (Dionex Ionpac AG 11), a self-regenerating suppressed conductivity detector (Dionex Ionpac ED50) and a gradient pump (Dionex Ionpac GP50). The detail procedures were given elsewhere (Yuan et al., 2003).

ACPD
12, 17151–17185, 2012

2.4.2 Element analysis

Half of each sample and blank filter was digested at 170 °C for 4 h in high-pressure Teflon digestion vessel with 3ml concentrated HNO_3, 1 ml concentrated HCl, and 1ml concentrated HF. After cooling, the solutions were dried, and then diluted to 10 ml with distilled deionized water. Total 24 elements (Al, Fe, Mn, Mg, Mo, Ti, Sc, Na, Ba, Sr, Sb, Ca, Co, Ni, Cu, Ge, Pb, P, K, Zn, Cd, V, S, and As) were measured by using an inductively coupled plasma atomic emission spectroscopy (ICP-OES; SPECTRO, Germany). The detailed analytical procedures were given elsewhere (Sun et al., 2004; Zhuang et al., 2001).

2.4.3 Carbonaceous aerosol analysis

Quartz filters were pre-heated at 500° for 5 h before using and the samples were analyzed for OC/EC using DRI Model 2001 (Thermal/Optical Carbon Analyzer). The IMPROVE thermal/optical reflectance (TOR) protocol (Chow and Watson, 2002) was used for the carbon analysis. The eight fractions (OC1, OC2, OC3, OC4 at 120, 250, 450 and 550 °C, respectively in a helium atmosphere, EC1, EC2, EC3 at 550, 700 and 800 °C, respectively, in the 98 % helium/2 % oxygen atmosphere) and OPC (optically detected pyrolized carbon) were measured separately. The IMPROVE protocol defined OC as OC1 + OC2 + OC3 + OC4 + OPC and EC as EC1 + EC2 + EC3–OPC.

3 Results and discussion

3.1 Air pollution during the Chinese Spring Festival season

One intensive atmospheric field campaign was carried out in an Eastern China megacity, Shanghai. The study period lasted from 15 January to 12 February in 2009, which just covered one of the most important Chinese traditional festivals, the Chinese Spring Festival. The average concentrations of $PM_{2.5}$ and PM_{10} during the study period were

ACPD
12, 17151–17185, 2012

61.5 ± 47.3 and 89.8 ± 53.1 μg m^{-3}, respectively. $PM_{2.5}$ accounted for a dominant fraction of 68.5 % in PM_{10}, indicating that fine particle was the main source of aerosol in Shanghai. Figure 1 shows the times series of hourly $PM_{2.5}$, PM_{10} concentrations, aerosol scattering (σ_{sp}) and absorbing coefficient (σ_{ap}), and single scattering albedo (ω) during the study period. Also, meteorological parameters are shown in the same figure, including hourly wind speed/direction, relatively humidity, rainfall amount and visibility. There were several pollution episodes based on the particle concentration and visibility. The first pollution episode occurred from 16–18 January with average visibility of 4.1 ± 2.2 km. The average $PM_{2.5}$ and PM_{10} concentration reached 85.4 ± 33.2 and 142.5 ± 26.2 μg m^{-3}, respectively. Correspondingly high aerosol scattering coefficient (σ_{sp}) also occurred with mean value of 297.2 ± 189.8 M m^{-1} as shown in Fig. 1e. As stated in the introduction section, the spring travel rush usually started about 1–2 weeks before the Chinese Lunar New Year. During this period, most of the immigrant residents in Shanghai started traveling back to their born places for the reunion of their families. Agencies in companies, industries and government usually gave their employees the holiday leave about a week before the holiday. Most people intended to travel during this period, thus the week before the Spring Festival was the busiest period for the transportation system, including the road vehicles, railways and airlines. To fit the increasing demands of transportation resources, hundreds of thousands of temporary buses and trains were operated. The average aerosol absorption coefficient (σ_{ap}) during this period reached 99.1 ± 64.1 M m^{-1}, corresponding to the black carbon (BC) concentration of 8.5 μg m^{-3}, which was the highest during the study period. This extremely high BC concentration corroborated the effect of spring travel rush on the air pollution as stated above. Consequently, the average single scattering albedo (ω), which was defined as the ratio of σ_{sp} to the total aerosol extinction coefficient ($\sigma_{sp} + \sigma_{ap}$), reached extremely low value of 0.70, indicative of large release of fresh combustion aerosol. Figure 2 shows the time series of hourly gaseous concentrations, including NO_x ($NO + NO_2$), CO, SO_2 and O_3. As the major gases emitted from vehicle exhaust, NO_x and CO evidently presented the highest concentrations during

ACPD
12, 17151–17185, 2012

this pollution episode. The average NO_x and CO concentration reached remarkably high concentrations of 270 and 2572 $\mu g\,m^{-3}$, respectively, indicating the significantly strengthened vehicle emission. During this period, the relative humidity was at moderate level of about 70 %. Wind speeds maintained around 1.0 $m\,s^{-1}$ and sometimes were stagnant (Fig. 1). This typical stagnant synoptic meteorology favored the local atmospheric processing and accumulation of pollutants. As this pollution occurred before the Spring Festival, we denoted it as the "pre-holiday pollution episode".

In the following several days, the aerosol concentrations had obvious decreases, which were partly due to the increased wind speeds that favored the diffusion of pollutants and partly due to several precipitation events as shown in Fig. 1. Extremely high particle concentrations occurred on 25 and 26 January, which were exactly the Chinese Lunar New Year's Eve and Lunar New Year's Day. Particle concentrations started to rise from 19:00 LST (Local Standard Time) on the 25 January and remained at high levels for about 16 h to 10:00 LST on the 26 January 2009 (Fig. 1d). The hourly peaks climbed to over 900 $\mu g\,m^{-3}$ between 00:00–01:00 LST on the 26th, which was almost $10 \sim 20$ times that of the normal periods. Correspondingly, the peak value of hourly σ_{sp} reached extreme value of 807.2 $M\,m^{-1}$. Also, some pollution gases such as SO_2 and NO_x reached very high levels of 438 and 286 $\mu g\,m^{-3}$, respectively. The intensive and widespread burning of fireworks were responsible for this burst of heavy pollution as all the residents were celebrating the national holiday at the same time. The average visibility was 4.9 km and we denoted this period as the "holiday pollution episode". Afterwards, particle concentrations dropped a lot, probably due to the substantial decrease of fireworks burning.

After the seven-day national holiday, aerosol pollution started to rise from 31 January and persisted till 11 February. As visualized in Fig. 1, obviously increasing trends of PM concentrations and σ_{sp} were observed during this period on a daily basis. Correspondingly, some pollution gases, i.e. CO, SO_2, and NO_x also had similar temporal patterns as shown in Fig. 2. We attributed this to another peak transport rush period after the national holiday, when people from the other provinces and cities started to go back

ACPD
12, 17151–17185, 2012

Shanghai for working and studying. The day-by-day increased passenger flows were reflected by the change of anthropogenic activities, such as increased usage of domestic and industrial electricity (e.g. SO_2) and more demand of transportation system (e.g. NO_x and CO). Compared to the pre-holiday pollution, the particle concentration was lower with average $PM_{2.5}$ and PM_{10} concentrations of 67.7 and 97.5 $\mu g\,m^{-3}$, respectively. σ_{sp} of this period averaged $283.2 \pm 121.6\,Mm^{-1}$, close to the pre-holiday pollution episode. However, σ_{ap} was much lower ($48.1 \pm 15.8\,Mm^{-1}$) and almost half of the pre-holiday pollution episode. We explained that people had relatively flexible traveling schedule after the festival compared to the stringent schedule before the festival. Daily traffic emissions were probably not as strong as before, which explained the much lower σ_{ap}, NO_x (NO, NO_2), and CO levels. Visibility reached the lowest during the whole study period with mean value of 2.96 ± 1.77 km. Relative high humidity (Fig. 1a) was one of the important factors accounting for the low visibility. We denoted this pollution episode as the "post-holiday pollution episode".

3.2 Diurnal variation

Diurnal variations of various atmospheric parameters are shown in Fig. 3. NO_x and CO were both major gases from vehicle exhausts, showing their first peaks from around 6:00 to 9:00 LST. This corresponded to the morning rush hours when there were large flows of people going for working and studying. Additionally, high emission diesel vehicles and heavy trucks from outside the Shanghai city usually operated in the morning times and could further contribute to this morning intensive pollution episodes. In the early morning, temperature was relatively low and the boundary layer hadn't been fully developed. Thus, air pollutants were likely trapped to some extent. Afterwards, vehicle emissions gradually decreased. In addition, as the temperature and sun radiation started to increase and the boundary layer developed, stronger atmospheric convection was expected than the early morning. Hence, the air pollutant concentrations had obvious decreases from 10:00 to 16:00 LST. Besides, we found the wind speeds of this

ACPD
12, 17151–17185, 2012

period were relatively higher (~2.1 m s^{-1}) than the other periods of time (~1.1 m s^{-1}), which also facilitated the dispersion of particles. After 16:00, the sun radiation began to decrease. The height of the mixing layer lowered correspondingly and the inversion began to form, which reduced the ability of air diffusion while instead trapped the pollutants in the lower atmosphere. Along with the gradually enhanced vehicle emission, the second peak of NO_x and CO was observed during the evening rush hours from around 17:00 to 20:00 LST. Most extremes occurred during the rush hours (see outliers in the figure), reflecting the greatly varying amplitude of vehicle emission source. As for O_3 (Fig. 3c), its diurnal pattern varied oppositely to that of NO_x and CO, which peaked around noon while troughs occurred during morning and evening rush hours. As Shanghai was in the VOC-limited regime (Geng et al., 2008, 2009; Ran et al., 2009), the titration effect of nitrogen oxides on O_3 was its major sink: $O_3 + NO \rightarrow O_2 + NO_2$, $NO_2 + NO \rightarrow NO_x$. Thus, the concentration of O_3 was depressed when the emission of NO was most intense during the rush hours. Around noon, the sun radiation strengthened a lot and NO_2 could be easily decomposed to form O_3. The diurnal pattern of SO_2 differed from any of the other gases as shown in Fig. 3d. As coal burning was the major source of SO_2 in Shanghai, vehicle emission evidently had negligible effects on its concentration during the rush hours. The lowest concentrations of SO_2 occurred during midnight around 23:00 to 6:00. Human activities were the lowest during this period, the decreased demand of electricity usage should be responsible for the low SO_2 concentrations. During the daytime, SO_2 gradually increased and peaked around noon, probably due to increased demand of electricity power such as from industries, companies and other facilities. Afterwards, SO_2 didn't fluctuate very much and stayed at a certain level, indicating relatively stable SO_2 emission sources.

The diurnal pattern of $PM_{2.5}$ resembled that of NO_x and CO to certain extent, which also showed peaks in both the morning and evening rush hours, indicating the significant impact of vehicle emission on particle formation. However, the diurnal variation of $PM_{2.5}$ was not as distinct as that of NO_x and CO as shown in the figure. For instance, $PM_{2.5}$ concentrations around noon were very close to the levels of the morning rush

ACPD
12, 17151–17185, 2012

hours. We attributed this to the contribution of sulfate aerosol from its precursor SO_2. The diurnal variation of aerosol scattering coefficient (σ_{sp}) resembled that of $PM_{2.5}$. These two parameters had a significant linear relation with correlation coefficient of 0.76 during the study period, indicating major aerosol components were light scattering. The diurnal variation of the aerosol absorbing coefficient (σ_{ap}) showed similar pattern as NO_x and CO (Fig. 3g). σ_{ap} moderately correlated with NO_x and CO with correlation coefficients of 0.63 and 0.71, respectively, while it only weakly correlated with SO_2 with correlation coefficient of 0.48. This suggested that mobile emission dominated the source of the light-absorbing substances (i.e. black carbon) more than the stationary emission. As expected, the single scattering albedo (ω) mirrored the diurnal cycle of σ_{ap} and showed two troughs during the morning and evening rush hours. The average ω_0 was 0.77 during the rush hours, suggesting strong fresh combustion aerosol. The extremely low ω_0 values and high BC concentrations indicated that vehicle emission had been an important source of air pollutants and should be seriously considered and regulated due to its warming effect of the atmosphere. As a consequence, a clear diurnal pattern of visibility showed consistence with the intensity of vehicle emission. During the rush hours, the average visibility was as low as 5.3 km. Even in the non-rush times, the average visibility was only 5.8 km, which was far below the haze criteria of 10 km. This indicated that during the Spring Festival traveling season, traffic emission was a major source of air pollution and greatly deteriorated the air quality in Shanghai.

3.3 Chemical signatures for pollution identification

3.3.1 Elemental concentration levels and source apportionment

Totally 31 elements were measured and analyzed in this study, and their average concentrations with one standard deviation in $PM_{2.5}$ and TSP are summarized in Table 1. Of all the elements, sulfur (S) had the highest concentration with mean values of 4.12 ± 3.26 and $6.04 \pm 4.36\,\mu g\,m^{-3}$ in $PM_{2.5}$ and TSP, respectively. Sulfur mainly

ACPD
12, 17151–17185, 2012

derived from the usage of coal and it indicated coal combustion was still a major component of air pollution in Shanghai. Al and Ca ranked the second and third among all the elements. Compared to the previous results of 2004 and 2005 in Shanghai (Wang et al., 2006), their concentrations in this study were a factor of 2–5 lower. The reason could be that, on the one hand, emission from construction activities were more effectively controlled due to the forthcoming 2010 Shanghai World Expo. Various measures were implemented to reduce construction and roadside dust pollution, including requirements on the covering or containment of idle soil, cement, and construction waste (UNEP, 2009). On the other hand, due to the long vacation during the Spring Festival, most of the construction sites were temporarily shutdown. By using the formula proposed by (Malm et al., 1994), the mineral concentration could be calculated as [Minerals] = 2.2[Al] + 2.49[Si] + 1.63[Ca] + 2.42[Fe] + 1.94[Ti], and it accounted for about 12.0 % and 27.7 % to $PM_{2.5}$ and TSP mass, respectively. Thus, minerals contributed a minor part to the aerosol, especially in fine particles.

Enrichment degrees of elements could be assessed by using the enrichment factors (EF) analysis: $EF = (X/X_{Ref})_{aerosol}/(X/X_{Ref})_{crust}$, where X was the element of interest and X_{Ref} was the reference element with Al chosen in this study. Elements with EFs less than 10 were usually regarded mainly derived from natural sources, which included Al, Ca, Fe, Mg, Na, Sc, and P in this study. Elements with EFs in the range of $10 \sim 100$ included Sr, Mn, K, Ti, V, Ba, Ni, Cr, Cu, and Mo, which suggested that these elements were moderately contaminated. The remaining elements had EFs around or even higher than 1000. The average EFs of Pb, Zn, Cd, As, Sb, S, and Se were 765, 936, 1258, 2431, 2793, 7552, and 8888, respectively, indicating that they were highly contaminated.

In order to further characterize the sources of elements, the principle component analysis (PCA) was applied by using the rotated component matrix. The results are shown in Table 2 and five factors were extracted from the whole dataset, which could totally explain 83.17 % of the variance, suggesting most of the sources have been explained. The first factor (PC1) could explain 18.16 % of the total variance and showed

ACPD
12, 17151–17185, 2012

high loadings for Al, Ca, Mg, Na, Ti and moderate loading for Fe. This factor obviously represented the natural source. The second factor (PC2) with a variation of 18.39 % showed high loadings for Co, Cr, Fe, Mn, Mo, and Ni, and we attributed this factor to the vehicular emission which emitted these trace metals through braking process and exhaust releases (Amato et al., 2009). The third factor (PC3) had a high loading for Ba, Cu, K, and Sr, and a moderate loading for Pb, which could explain 17.96 % of the variance. At normal times, these metals derived from miscellaneous sources. As this study covered the most intense fireworks burning episodes, theses metals were probably derived from the burning of fireworks as they are usually used as additives in fireworks. Previous results on the Lantern Festival in Beijing also revealed that theses metals increased substantially due to the fireworks burning (Wang et al., 2007). The fourth factor (PC4) showed high loadings for Cd, Pb, Sb, and Se and could explain 15.89 % of the variance. These elements probably came from the industrial and metallurgical emission. Pb in Shanghai had the major source from traffic emission in early years, while coal combustion had dominated the lead pollution after the phasing out of leaded gasoline since 1997 (Chen et al., 2005; Tan et al., 2006; Zhang et al., 2009b). The last factor (PC5) had significant loadings for As, Ge, S, and Se, which evidently dervied from coal burning. Se and SO_4^{2-} had significant correlation ($R = 0.76$) as shown in Fig. 5a. The extremely high enrichment of Se suggested that coal burning was a significant source of air pollution in Shanghai.

3.3.2 Pollution process analysis

Figure 4 presented the time-series of daily SO_4^{2-}, NO_3^-, NH_4^+, and organic carbon (OC) concentrations in $PM_{2.5}$ during the study period. During the pre-holiday pollution episode (16–18 January), the secondary inorganic species were at moderate levels. SO_4^{2-}, NO_3^-, and NH_4^+ averaged 5.3, 7.2, and 5.5 $\mu g\,m^{-3}$, respectively. The biggest contributor to aerosol was OC, which averaged 13.7 $\mu g\,m^{-3}$ and showed the highest during the whole period. If we applied an OM/OC ratio of 2.0 to estimate the mass

ACPD
12, 17151–17185, 2012

of organic matter (OM) (Turpin and Lim, 2001), the average mass contribution of OM to $PM_{2.5}$ could be as high as 44.6 %. As discussed in Sect. 3.1, we have mainly attributed this pollution episode to the enhanced vehicle emission. Figure 5b shows the linear correlation between OC and CO, and their significant correlation ($R = 0.71$) corroborated the impact of vehicle emission on the first pollution episode. In the following days from 19 to 24 January, all the chemical species stayed at relatively low levels. As discussed above, favorable meteorological conditions, e.g. higher wind speed and more precipitation, played an important role. During the holiday pollution episode (25–26 January), OC concentration had risen up almost one fold compared to the previous days (19–24 January), with the average concentration of 11.5 $\mu g\,m^{-3}$. While the secondary inorganic species remained low with 3.7, 1.7, and 3.5 $\mu g\,m^{-3}$ for SO_4^{2-}, NO_3^-, and NH_4^+, respectively. We speculated that the remaining part of aerosol derived from the fireworks burning, which were mainly in the form of oxidation states of metals used for additives in fireworks. During the post-holiday episode (31 January–10 Feburary), organic aerosol was at moderate level while the secondary inorganic species reached the highest levels during the study period. SO_4^{2-}, NO_3^-, and NH_4^+ averaged 19.2, 10.2, and 13.4 $\mu g\,m^{-3}$, respectively. The sum of these three species accounted for a dominant fraction of 74 % in $PM_{2.5}$. Consistent with the temporal variation of aerosol concentrations, aerosol scattering coefficient and pollutant gases (Fig. 1 and 2), SO_4^{2-}, NO_3^-, and NH_4^+ also exhibited an increasing trend during the post-holiday episode. This day-to-day pattern reflected that vehicular and industrial emissions had gradually increased probably due to growth of human flows from other regions outside Shanghai and most industries started to re-open. It was noted that the NH_4^+ concentration during the post-holiday pollution episode was 3–4 times higher than the other times. The increased NH_4^+ was attributed to the anthropogenic activities, such as vehicular exhausts, human excrement, burning of agriculture straws and etc. NH_4^+ was a major alkaline component for neutralizing the acids. As shown in Fig. 5c, d, the equivalent NH_4^+ concentration had a perfect linear correlation ($R > 0.90$) with the sum of SO_4^{2-} and NO_3^- equivalent concentrations in both $PM_{2.5}$ and TSP. And the slopes between

ACPD
12, 17151–17185, 2012

NH_4^+ versus $[SO_4^{2-} + NO_3^-]$ were close or slightly higher than 1.0, indicating the complete neutralization. Thus, the enhancement of ammonium was the major cause for the increase of sulfate and nitrate. In the most polluted areas in China such as NCP (North China Plain), and YRD (Yangtze River Delta), NH_3 was sufficiently abundant. The 90 % increase of NH_3 emissions during 1990–2005 resulted in ~50–60 % increases of NO_3^- and SO_4^{2-} aerosol concentrations (Wang et al., 2011). It was suggested that the most effective pathway to mitigate air pollution was to adopt a multi-pollutant strategy to control NH_3 emissions in parallel with current SO_2 and NO_x controls in China.

3.4 Factors affecting the visibility impairment

3.4.1 Role of ambient water vapor

Figure 6 shows the scatter plot between hourly visibility and $PM_{2.5}$ concentration grouped by the corresponding relatively humidity (RH). The data with precipitation events and intense events of fireworks burning were excluded to avoid the statistical analysis of extreme values. Generally, the two parameters presented a negative relationship but it was nonlinear. If we used a threshold of visibility = 10 km to distinguish between haze and non-haze weather, it could be visually seen that the non-haze events (i.e. visibility ≥ 10 km) were usually accompanied with $PM_{2.5}$ concentrations lower than 65 $\mu g\,m^{-3}$. It was also noted that the non-haze episodes usually had relatively low humidity. While for the haze events (i.e. visibility < 10 km), $PM_{2.5}$ concentrations fluctuated in a wide range, and the relative humidity (~80 %) was much higher than the non-haze events. As visualized in the figure, for a fixed visibility, $PM_{2.5}$ concentration with higher RH was lower than that with lower RH. In other words, at higher RH the atmospheric visibility should be more easily impaired by aerosol. This phenomenon was related to the dependence of aerosol scattering efficiency on the ambient water content. Major aerosol components, such as sulfate, nitrate, and ammonium were highly hygroscopic.

ACPD
12, 17151–17185, 2012

When RH increased, the aerosol scattering efficiency would exponentially increase (Day and Malm, 2001).

To quantitatively investigate the impact of ambient water vapor on the atmospheric visibility, we compared the visibility measured by a visibility ambient light sensor and the calculated visibility estimated from the aerosol scattering and absorption coefficient. Visibility had an inverse relationship with total extinction coefficient according to the Koschmieder formula

$$L_V = 3.912/b_{\text{ext}}, \quad (1)$$

where L_V was the visibility and the total extinction coefficient b_{ext} was due to scattering and absorption by particles and gases,

$$b_{\text{ext}} = b_{\text{sp}} + b_{\text{ap}} + b_{\text{sg}} + b_{\text{ag}} + b_{\text{sw}}. \quad (2)$$

Scattering (b_{sp}) and absorption coefficient (b_{ap}) by particles were measured by nephelometer and athelometor, respectively. Absorption of visible light by gases (b_{ag}) was considered to be essentially due to NO_2 and it could be estimated using the formula $\sigma_{\text{ag}} = 0.33 \times [NO_2]$ (Groblicki et al., 1981). Here, NO_2 was in units of $\times 10^{-9} V/V$. Rayleigh scattering coefficient (σ_{sg}) was assumed to be a constant of $0.013\,\text{km}^{-1}$ at sea level (Chan et al., 1999; Peundorf, 1957). And b_{sw} was the scattering coefficient of light due to moisture in the air, which was not measured in this study. We calculated the extinction coefficient without b_{sw} and then converted into visibility using Eq. (1). The calculated visibility was denoted as Vis_{cal} and the measured visibility was denoted as Vis_{mea}. Figure 6b shows the scatter plot between Vis_{cal} and Vis_{mea}. The two parameters were closely correlated with correlation coefficient of 0.77. However, the measured and calculated visibility had great discrepancy as indicated by the regression slope of $\text{Vis}_{\text{cal}}/\text{Vis}_{\text{mea}} = 1.4$. This indicated that there must be other parameter contributing to the total extinction. As we calculated the visibility without adding b_{sw}, we believed that this discrepancy between the measured and calculated values should be due to the

ACPD
12, 17151–17185, 2012

ambient water vapor. b_{sw} could be neglected when relatively humidity (RH) was lower than 70 % (Cass, 1979; Chan et al., 1999), while in this study the average relative humidity during the whole study period reached over 75 % and it exceeded 80 % during the post-holiday pollution episode as inferred in Sect. 3.1. Shanghai is costal city and its climate is humid with over 70 % RH all year around (Wang et al., 2006). Thus, it was not proper to excluded b_{sw} out of the calculation of the total extinction and this could explain the overestimated visibility. Based on the regression slope in Fig. 6b and Eq. (1), we could estimate that the contribution of water vapor to the visibility impairment was about 50 %. On the one hand, the high humidity caused considerable light extinction due to itself. On the other hand, the high humidity could make some hygroscopic components (e.g. sulfate ammonium, nitrate ammonium) become larger and more efficiently scattered light. Previous studies showed that the contribution of water content to the total sunlight scattering could be over 40 % at one background site in the Yangtze River Delta region (Xu et al., 2002), and also around 40 % at one site in the Pearl River Delta region with 80 % RH (Cheng et al., 2008a). Even in Beijing, the contribution of water vapor could reached 25 % in summer (Zhang et al., 2010). In this study, the role of ambient water vapor on light extinction was higher than the above studies, which should be due to the higher RH in this study.

3.4.2 Aerosol optical properties apportioned to chemical composition

In this section, the contribution of different chemical composition to the aerosol extinction was quantified. Aerosol was categorized into six groups, i.e. sulfate ammonium, nitrate ammonium, organic aerosol, elemental carbon, dust, and sea salt. As shown in Fig. 5, the equivalent ratio of NH_4^+ versus the sum of SO_4^{2-} and NO_3^- was close to 1.00. Thus, the concentration of sulfate ammonium and nitrate ammonium could be estimated using the formula: $m[(NH_4)_2SO_4] = m[SO_4^{2-}] \cdot (1 + 18*2/96)$, $[NH_4NO_3] = m[NO_3^-] \cdot (1 + 18/62)$. Of which $m[SO_4^{2-}]$ and $m[NO_3^-]$ represented the mass concentration of SO_4^{2-} and NO_3^-, and 18, 96, and 62 represented the molecular weight

ACPD
12, 17151–17185, 2012

of NH_4^+, SO_4^{2-}, and NO_3^-, respectively. Organic aerosol (OA) was estimated by applying an OM/OC ratio of 2.0 (Turpin and Lim, 2001). Estimation of sea salts assumed all the measured Na^+ was derived from the marine source, and the sea salts were estimated using [sea salt] = $[Na^+] + [Na^+] \cdot 2.645$. Here, 2.645 was the seawater mass ratio of the other ions (Cl^-, SO_4^{2-}, Ca^{2+}, Mg^{2+}, K^+) to Na^+. The estimation of dust aerosol had been stated in Sect. 3.3.1. As no scattering and absorption efficiencies of chemical species in the Yangtze River Delta region were reported yet, we adopted these parameters that were investigated in the Pearl River Delta region (Table 3 in Cheng et al., 2008b). Figure 7 shows the fractional contributions of major chemical composition to the aerosol scattering and absorption during the whole study period. It was found that the whole study period could be divided into two periods. From 15 to 26 January, the aerosol scattering was dominated by the organic aerosol and its average contribution to the aerosol scattering reached 59 % during this period. Except for the pre-holiday pollution episode when the traffic emission dominated, the other low PM periods were also dominated by the organic aerosol. This indicated that organic aerosol had served as an important background aerosol component in Shanghai. Since 27 January, the contribution from inorganic components to the aerosol scattering started to overwhelm that of organic aerosol. The average contribution of sulfate and nitrate reached about 69 %, while that of OA decreased to 26 %. Compared to the secondary inorganic and organic components, the contribution of EC, sea salt and dust to the aerosol scattering was much smaller, which totally contributed about 7 %. Figure 7b shows the fractional contributions of major chemical species to the aerosol absorption. Elemental carbon evidently dominated the absorption during the whole study, accounting for an average of over 90 % due to that EC had the strongest absorption efficiency. Although organic aerosol and dust also had absorptive effect, their magnitudes were significantly lower than that of EC. Finally, we summarized the contribution of major chemical species to the total aerosol extinction (scattering + absorbing) in Fig. 8. Organic aerosol had the largest contribution of 47 %, whose source we had discussed about could be mainly derived from the vehicle emission. The next two biggest contributors were sulfate ammonium

ACPD
12, 17151–17185, 2012

and nitrate ammonium, which contributed an average of 22 % and 14 %, respectively. Although EC only comprised about 2 ~ 5 % of the aerosol mass concentration, its contribution to the aerosol extinction was as high as 12 %, due to its highest extinction efficiency. From the results above, we could find that traffic-related species (i.e. OA, nitrate and EC) all had significant radiative effects, which highlight the importance of controlling vehicle numbers and emissions on the air pollution in mega-cities of China.

4 Conclusions

We initiated an intensive atmospheric campaign during the Chinese Spring Festival peak transportation season of 2009 in a Chinese megacity, Shanghai. Three pollution episodes dominated by different emission sources were identified prior to, during, and after the holiday, respectively. The spring travel rush before the holiday caused significantly enhanced vehicle emission as tremendous immigrant residents in Shanghai were traveling back to their born hometown. Black carbon reached the highest of 8.5 $\mu g\,m^{-3}$ during the whole study period with extreme low single scattering albedo of 0.70, indicating strong fresh combustion. Organic aerosol dominated with contribution of 45 % and 60 % to $PM_{2.5}$ mass and the total aerosol scattering, respectively. On the New Year's Eve and Day, aerosol mass, scattering coefficient, and pollution gases (e.g. SO_2, NO_x) peaked due to intense burning of fireworks for celebrating the Chinese New Year. After the holiday, the gradually increased emission due to spring travel rush resulted in increases of various pollutants. SO_4^{2-}, NO_3^-, and NH_4^+ averaged 19.2, 10.2, and 13.4 $\mu g\,m^{-3}$, respectively, summing a dominant fraction of 74 % in $PM_{2.5}$. Principle component analysis on 31 elements apportioned five major sources, i.e. natural source, vehicular emission, burning of fireworks, industrial and metallurgical emission, and coal burning. Correlation between $PM_{2.5}$ and visibility indicated higher relative humidity had tremendous acceleration on the visibility impairment. Comparison between the measured and calculated visibility estimated that the effect of ambient water vapor contributed as high as 50 % to the total light extinction. Among the total aerosol

ACPD
12, 17151–17185, 2012

extinction, organic aerosol contributed most of 47 %, followed by sulfate ammonium and nitrate ammonium with shares of 22 % and 14 %, respectively. Although black carbon only comprised about 2 ∼ 5 % of the aerosol mass, its contribution to the aerosol extinction was as high as 12 %. Overall, we found that traffic-related species (i.e. organics, nitrate and black carbon) all had significant radiative effects, which highlight the importance of controlling vehicle numbers and emissions on the air pollution in mega-cities of China.

Acknowledgements. This work was supported by the great international collaboration project of MOST, China (2010DFA92230), National Natural Science Foundation of China (Grant Nos. 41128005 (fund for collaboration with oversea scholars), 20877020, 20977017), and Shanghai environmental protection science developing funding (No.2010-003).

References

Amato, F., Pandolfi, M., Viana, M., Querol, X., Alastuey, A., and Moreno, T.: Spatial and chemical patterns of PM_{10} in road dust deposited in urban environment, Atmos. Environ., 43, 1650–1659, 2009.

BBC: China's holiday rush begins early, http://news.bbc.co.uk/2/hi/asia-pacific/7813267.stm (last access: January 2009), 2009.

Cass, G. R.: On the relationship between sulfate air quality and visibility with examples in los angeles, Atmos. Environ., 13, 1069–1084, 1979.

Chan, C. K. and Yao, X.: Air pollution in mega cities in China, Atmos. Environ., 42, 1–42, 2008.

Chan, Y. C., Simpson, R. W., McTainsh, G. H., Vowles, P. D., Cohen, D. D., and Bailey, G. M.: Source apportionment of visibility degradation problems in Brisbane (Australia) using the multiple linear regression techniques, Atmos. Environ., 33, 3237–3250, 1999.

Che, W. W., Zheng, J. Y., Wang, S. S., Zhong, L. J., and Lau, A. I.: Assessment of motor vehicle emission control policies using Model-3/CMAQ model for the Pearl River Delta region, China, Atmos. Environ., 45, 1740–1751, 2011.

Chen, J. M., Tan, M. G., Li, Y. L., Zhang, Y. M., Lu, W. W., Tong, Y. P., Zhang, G. L., and Li, Y.: A lead isotope record of shanghai atmospheric lead emissions in total suspended particles during the period of phasing out of leaded gasoline, Atmos. Environ., 39, 1245–1253, 2005.

ACPD

12, 17151–17185, 2012

Cheng, Y. F., Wiedensohler, A., Eichler, H., Heintzenberg, J., Tesche, M., Ansmann, A., Wendisch, M., Su, H., Althausen, D., Herrmann, H., Gnauk, T., Bruggemann, E., Hu, M., and Zhang, Y. H.: Relative humidity dependence of aerosol optical properties and direct radiative forcing in the surface boundary layer at Xinken in Pearl River Delta of China: an observation based numerical study, Atmos. Environ., 42, 6373–6397, 2008a.

Cheng, Y. F., Wiedensohler, A., Eichler, H., Su, H., Gnauk, T., Brueggemann, E., Herrmann, H., Heintzenberg, J., Slanina, J., Tuch, T., Hu, M., and Zhang, Y. H.: Aerosol optical properties and related chemical apportionment at Xinken in Pearl River Delta of China, Atmos. Environ., 42, 6351–6372, 2008b.

Chow, J. C. and Watson, J. G.: $PM_{2.5}$ carbonate concentrations at regionally representative interagency monitoring of protected visual environment sites, J. Geophys. Res., 107, 8344, doi:10.1029/2001JD000574, 2002.

Day, D. E. and Malm, W. C.: Aerosol light scattering measurements as a function of relative humidity: a comparison between measurements made at three different sites, Atmos. Environ., 35, 5169–5176, 2001.

Geng, F. H., Tie, X. X., Xu, J. M., Zhou, G. Q., Peng, L., Gao, W., Tang, X., and Zhao, C. S.: Characterizations of ozone, NO_x, and VOCs measured in Shanghai, China, Atmos. Environ., 42, 6873–6883, 2008.

Geng, F. H., Zhang, Q., Tie, X. X., Huang, M. Y., Ma, X. C., Deng, Z. Z., Yu, Q., Quan, J. N., and Zhao, C. S.: Aircraft measurements of O_3, NO_x, CO, VOCs, and SO_2 in the Yangtze River Delta region, Atmos. Environ., 43, 584–593, 2009.

Groblicki, P. J., Wolff, G. T., and Countess, R. J.: Visibility-reducing species in the Denver Brown Cloud. 1. Relationships between extinction and chemical-composition, Atmos. Environ., 15, 2473–2484, 1981.

Lei, Y., Zhang, Q., He, K. B., and Streets, D. G.: Primary anthropogenic aerosol emission trends for China, 1990–2005, Atmos. Chem. Phys., 11, 931–954, doi:10.5194/acp-11-931-2011, 2011.

Magee-Scientific: The Aethalometer, Magee Scientific Company, Berkeley, California, USA, 2005.

Malm, W. C., Sisler, J. F., Huffman, D., Eldred, R. A., and Cahill, T. A.: Spatial and seasonal trends in particle concentration and optical extinction in the United States, J. Geophys. Res.-Atmos., 99, 1347–1370, 1994.

ACPD
12, 17151–17185, 2012

Peundorf, R.: Tables of the refractive index for standard and the Rayleigh scattering coefficient for the spectral region between 0.2 and 20.0 microns and their application to atmospheric optics, J. Opt. Soc. Am., 47, 176–182, 1957.

Ramana, M. V., Ramanathan, V., Feng, Y., Yoon, S. C., Kim, S. W., Carmichael, G. R., and Schauer, J. J.: Warming influenced by the ratio of black carbon to sulphate and the black-carbon source, Nat. Geosci., 3, 542–545, 2010.

Ran, L., Zhao, C. S., Geng, F. H., Tie, X. X., Tang, X., Peng, L., Zhou, G. Q., Yu, Q., Xu, J. M., and Guenther, A.: Ozone photochemical production in urban Shanghai, China: analysis based on ground level observations, J. Geophys. Res., 114, D15301, doi:10.1029/2008JD010752, 2009.

SMSB, Shanghai Municipal Statistics Bureau: Shanghai sixth national census in 2010 Communiqué on Major Data, Shanghai Municipal Statistics Bureau, available at: http://www.shanghai.gov.cn/shanghai/node2314/node2319/node12344/u26ai25463.html, 2011 (in Chinese).

Sun, Y. L., Zhuang, G. S., Ying, W., Han, L. H., Guo, J. H., Mo, D., Zhang, W. J., Wang, Z. F., and Hao, Z. P.: The air-borne particulate pollution in Beijing – concentration, composition, distribution and sources, Atmos. Environ., 38, 5991–6004, 2004.

Tan, M. G., Zhang, G. L., Li, X. L., Zhang, Y. X., Yue, W. S., Chen, J. M., Wang, Y. S., Li, A. G., Li, Y., Zhang, Y. M., and Shan, Z. C.: Comprehensive study of lead pollution in Shanghai by multiple techniques, Anal. Chem., 78, 8044–8050, 2006.

Turpin, B. J. and Lim, H. J.: Species contributions to $PM_{2.5}$ mass concentrations: revisiting common assumptions for estimating organic mass, Aerosol Sci. Tech., 35, 602–610, 2001.

UNEP: UNEP Environmental Assessment: Expo 2010 – Shanghai, China, United Nations Environment Programme, available at: http://www.unep.org/publications/contents/pub_details_search.asp?ID=4040, 2009.

USEPA: Quality assurance handbook for air pollution measurement systems, EPA – 454/R – 98 – 004, U.S. Environmental Protection Agency, Office of Air Quality Planning and Standards, Air Quality Assessment Division, Research Triangle Park, N.C., 1998.

van der A, R. J., Peters, D. H. M. U., Eskes, H., Boersma, K. F., Van Roozendael, M., De Smedt, I., and Kelder, H. M.: Detection of the trend and seasonal variation in tropospheric NO_2 over China, J. Geophys. Res., 111, D12317, doi:10.1029/2005JD006594, 2006.

ACPD
12, 17151–17185, 2012

Wang, Y., Zhuang, G. S., Zhang, X. Y., Huang, K., Xu, C., Tang, A. H., Chen, J. M., and An, Z. S.: The ion chemistry, seasonal cycle, and sources of $PM_{2.5}$ and TSP aerosol in Shanghai, Atmos. Environ., 40, 2935–2952, 2006.

Wang, Y., Zhuang, G. S., Xu, C., and An, Z. S.: The air pollution caused by the burning of fireworks during the lantern festival in Beijing, Atmos. Environ., 41, 417–431, 2007.

Wang, S. X., Zhao, M., Xing, J., Wu, Y., Zhou, Y., Lei, Y., He, K. B., Fu, L. X., and Hao, J. M.: Quantifying the air pollutants emission reduction during the 2008 Olympic Games in Beijing, Environ. Sci. Technol., 44, 2490–2496, 2010.

Wang, S. X., Xing, J., Jang, C., Zhu, Y., Fu, J. S., and Hao, J. M.: Impact assessment of ammonia emissions on inorganic aerosols in East China using response surface modeling technique, Environ. Sci. Technol., 45, 9293–9300, doi:10.1021/es2022347, 2011.

Xu, J., Bergin, M. H., Yu, X., Liu, G., Zhao, J., Carrico, C. M., and Baumann, K.: Measurement of aerosol chemical, physical and radiative properties in the Yangtze delta region of China, Atmos. Environ., 36, 161–173, 2002.

Yuan, H., Wang, Y., and Zhuang, G. S.: Simultaneous determination of organic acids, methanesulfonic acid and inorganic anions in aerosol and precipitation samples by ion chromatography, J. Instrum. Anal., 22, 11–44, 2003.

Zhang, Q., Streets, D. G., Carmichael, G. R., He, K. B., Huo, H., Kannari, A., Klimont, Z., Park, I. S., Reddy, S., Fu, J. S., Chen, D., Duan, L., Lei, Y., Wang, L. T., and Yao, Z. L.: Asian emissions in 2006 for the NASA INTEX-B mission, Atmos. Chem. Phys., 9, 5131–5153, doi:10.5194/acp-9-5131-2009, 2009a.

Zhang, Y. P., Wang, X. F., Chen, H., Yang, X., Chen, J. M., and Allen, J. O.: Source apportionment of lead-containing aerosol particles in Shanghai using single particle mass spectrometry, Chemosphere, 74, 501–507, 2009b.

Zhang, Q. H., Zhang, J. P., and Xue, H. W.: The challenge of improving visibility in Beijing, Atmos. Chem. Phys., 10, 7821–7827, doi:10.5194/acp-10-7821-2010, 2010.

Zhao, Y., Wang, S. X., Duan, L., Lei, Y., Cao, P. F., and Hao, J. M.: Primary air pollutant emissions of coal-fired power plants in China: current status and future prediction, Atmos. Environ., 42, 8442–8452, 2008.

Zhuang, G. S., Guo, J. H., Yuan, H., and Zhao, C. Y.: The compositions, sources, and size distribution of the dust storm from China in spring of 2000 and its impact on the global environment, Chinese Sci. Bull., 46, 895–901, 2001.

ACPD

12, 17151–17185, 2012

Table 1. Average concentration of elements with one standard deviation ($\mu g\,m^{-3}$) in $PM_{2.5}$ and TSP.

Elements	$PM_{2.5}$		TSP	
	Average	S.D.	Average	S.D.
Al	0.64	0.78	2.51	1.62
As	0.019	0.007	0.018	0.009
Ba	0.09	0.25	0.14	0.20
Br	BDL	BDL	0.01	0.01
Ca	0.72	0.78	3.39	1.63
Cd	8.98×10^{-4}	5.57×10^{-4}	1.10×10^{-3}	9.74×10^{-4}
Ce	1.70×10^{-3}	6.47×10^{-3}	1.71×10^{-2}	2.14×10^{-2}
Co	4.15×10^{-4}	4.66×10^{-4}	BDL	BDL
Cr	0.02	0.06	0.02	0.02
Cu	0.04	0.02	0.07	0.09
Eu	2.29×10^{-4}	6.71×10^{-4}	5.59×10^{-3}	8.88×10^{-3}
Fe	0.56	0.50	1.93	1.07
Ge	0.01	0.01	BDL	BDL
I	BDL	BDL	BDL	BDL
K	1.01	1.31	1.80	1.47
Mg	0.26	0.27	0.81	0.62
Mg	0.26	0.28	0.82	0.66
Mn	0.04	0.04	0.07	0.04
Mo	7.11×10^{-4}	5.61×10^{-4}	1.02×10^{-3}	1.09×10^{-3}
Na	0.45	0.40	1.73	1.04
Ni	0.01	0.02	0.01	0.01
P	0.003	0.02	0.04	0.07
Pb	0.06	0.04	0.11	0.21
S	4.12	3.26	6.04	4.36
Sb	3.06×10^{-3}	2.57×10^{-3}	4.46×10^{-3}	6.38×10^{-3}
Sc	6.38×10^{-5}	6.44×10^{-5}	6.67×10^{-5}	1.26×10^{-4}
Se	2.00×10^{-3}	1.60×10^{-3}	6.57×10^{-4}	9.84×10^{-4}
Sr	0.02	0.03	0.06	0.17
Ti	0.32	0.26	1.10	0.73
V	0.01	0.01	0.01	0.01
Zn	0.13	0.28	0.50	0.65

S.D.: standard deviation.
BDL: below detection limit.

ACPD
12, 17151–17185, 2012

Table 2. Principle component analysis of the major elements.

	Rotated component matrix				
Factor	PC1	PC2	PC3	PC4	PC5
Al	**0.63**	−0.04	0.58	0.16	−0.35
As	−0.09	0.10	0.33	−0.02	**0.85**
Ba	0.02	−0.08	**0.95**	0.00	0.05
Ca	**0.90**	0.04	0.22	0.02	−0.30
Cd	0.03	−0.04	0.04	**0.83**	0.34
Co	0.12	**0.95**	−0.01	0.11	0.07
Cr	−0.16	**0.95**	0.05	−0.21	−0.07
Cu	0.25	0.19	**0.62**	0.26	0.04
Eu	0.21	−0.09	0.48	−0.39	−0.35
Fe	**0.57**	**0.72**	0.11	0.14	−0.17
Ge	−0.02	0.12	0.04	0.34	**0.85**
K	0.00	0.03	**0.92**	0.17	0.30
Mg	**0.74**	0.00	0.56	−0.12	−0.03
Mn	0.30	**0.85**	−0.06	0.25	0.05
Mo	0.16	**0.65**	−0.13	0.59	0.20
Na	**0.87**	0.01	0.05	−0.18	0.15
Ni	−0.11	**0.97**	−0.06	−0.13	0.05
Pb	0.06	−0.10	**0.56**	**0.73**	0.26
S	−0.02	−0.11	0.00	0.32	**0.75**
Sb	0.21	0.14	0.08	**0.83**	0.09
Sc	0.59	0.07	0.04	0.59	−0.11
Se	−0.13	−0.06	0.13	**0.70**	**0.57**
Sr	0.12	−0.09	**0.95**	0.00	0.10
Ti	**0.82**	0.10	0.09	0.36	−0.12
V	0.58	0.22	−0.17	0.27	0.28
% of Variance	18.16	18.39	17.96	15.89	12.77

ACPD
12, 17151–17185, 2012

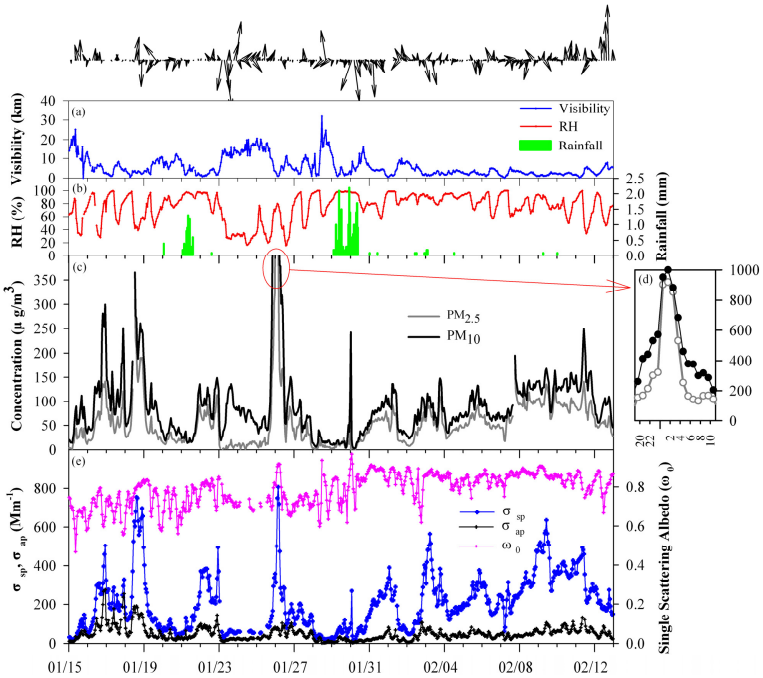

Fig. 1. Time-series of meteorological conditions and various aerosol parameters with time resolution of 1 h from 15 January to 12 February 2009 in Shanghai. **(a)** Wind speed/direction and visibility **(b)** relatively humidity (RH) and rainfall **(c)** $PM_{2.5}$ and PM_{10} mass concentration during the whole study period **(d)** $PM_{2.5}$ and PM_{10} mass concentration on the Chinese Lunar New Year's Eve (25 January) and the Chinese Lunar New Year's Day (26 January) **(e)** aerosol scattering coefficient (σ_{sp}), absorption coefficient (σ_{ap}) and single scattering albedo (ω_0).

ACPD
12, 17151–17185, 2012

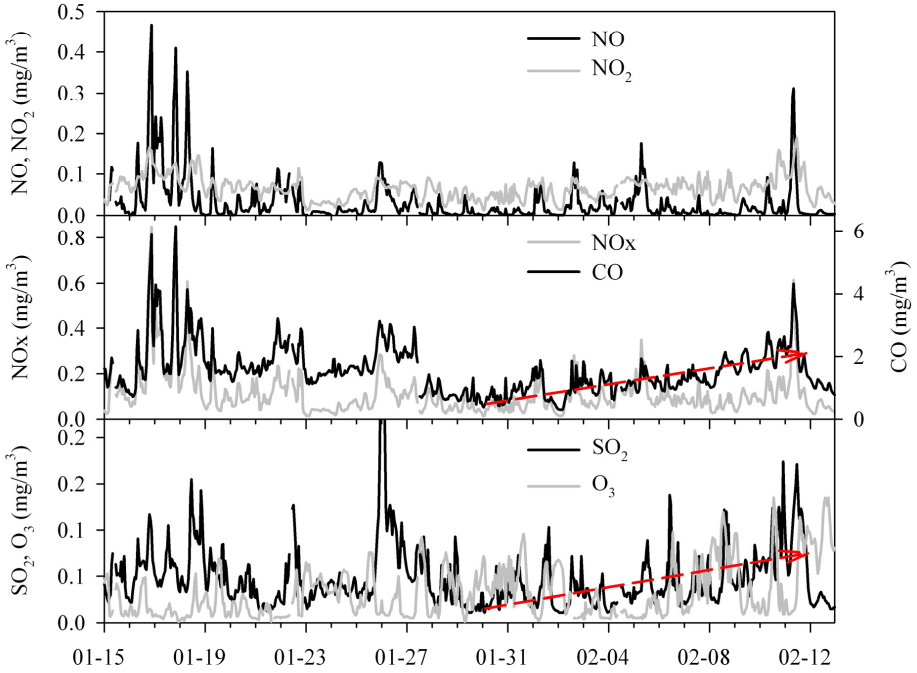

Fig. 2. Time-series of hourly NO_x ($NO + NO_2$), CO, SO_2 and O_3 concentrations. The dashed arrow lines denote the trends of CO and SO_2 concentrations during the post-holiday pollution episode from 31 January to 11 February.

ACPD
12, 17151–17185, 2012

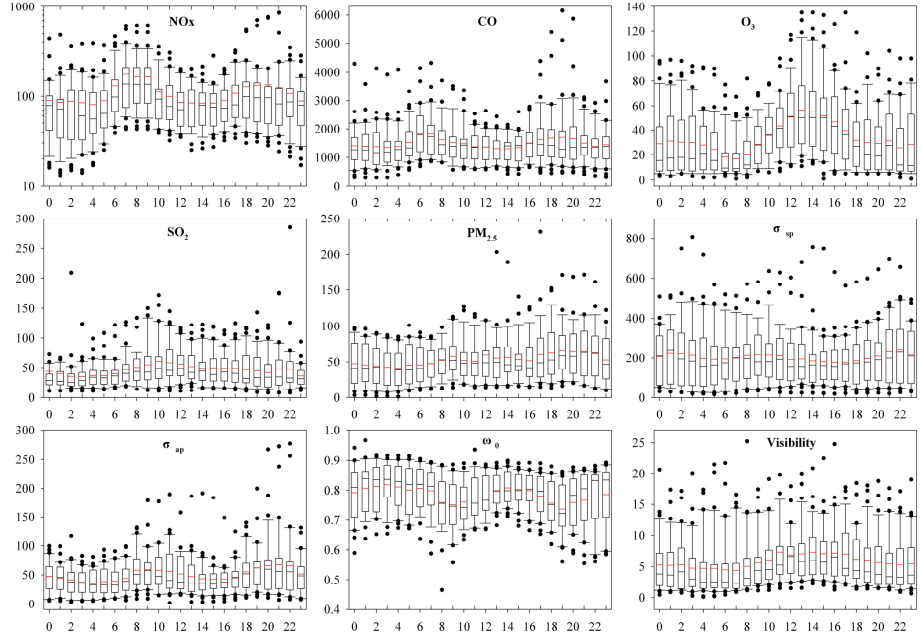

Fig. 3. Diurnal variation of NO_x, CO, O_3, SO_2, and $PM_{2.5}$ concentrations ($\mu g\,m^{-3}$), σ_{sp} and σ_{ap} ($M\,m^{-1}$), ω_0 (no units), and visibility (km). Bottom and top of the boxes represent the 25 and 75 % limits, respectively; and bottom and top short lines represent the minimum and maximum values, respectively; black and red lines inside boxes represent the median and mean values; black dots represent the outliers.

ACPD
12, 17151–17185, 2012

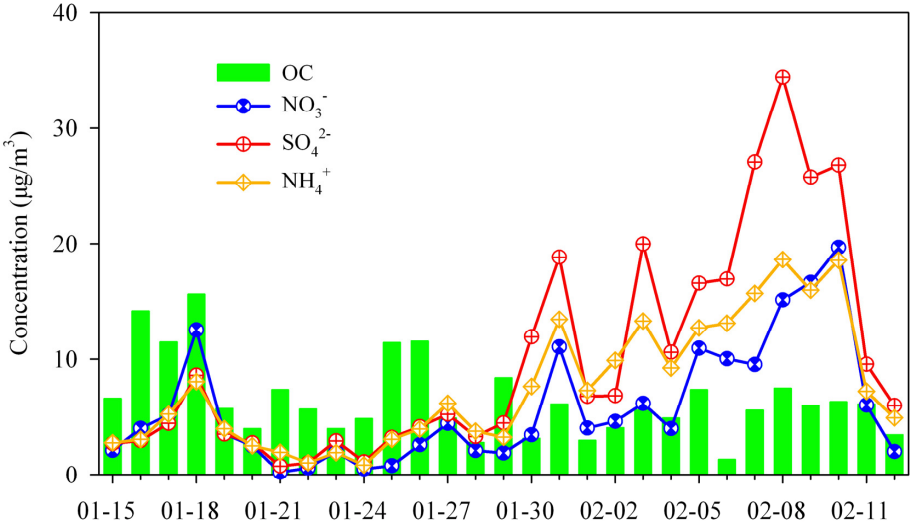

Fig. 4. Time-series of daily OC, NO_3^-, SO_4^{2-}, and NH_4^+ concentrations ($\mu g\,m^{-3}$) during the study period.

ACPD
12, 17151–17185, 2012

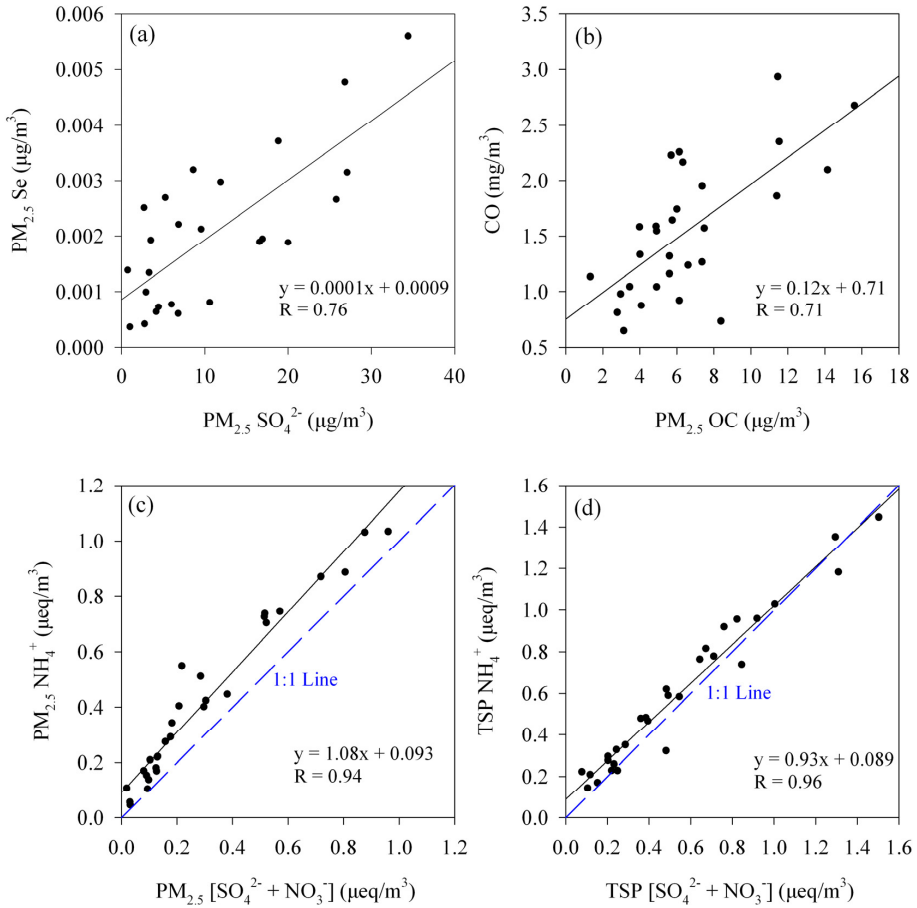

Fig. 5. The linear correlation between **(a)** Se and SO_4^{2-} in $PM_{2.5}$ **(b)** CO and $PM_{2.5}$ OC **(c)** the equivalent NH_4^+ concentration and the sum of equivalent SO_4^{2-} and NO_3^- concentration in $PM_{2.5}$ and **(d)** TSP. The dashed blue line denotes the 1 : 1 line.

ACPD
12, 17151–17185, 2012

Anthropogenic emission on air-quality over a megacity

K. Huang et al.

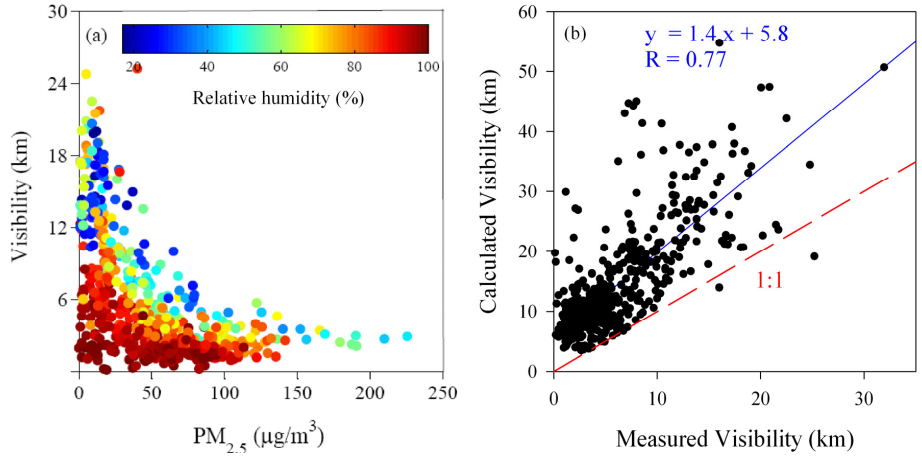

Fig. 6. (a) Scatter plot between hourly visibility and $PM_{2.5}$ concentration grouped by the corresponding relatively humidity **(b)** linear relationship between the measured and calculated visibility, the regression equation and 1 : 1 line are also shown in the figure.

ACPD
12, 17151–17185, 2012

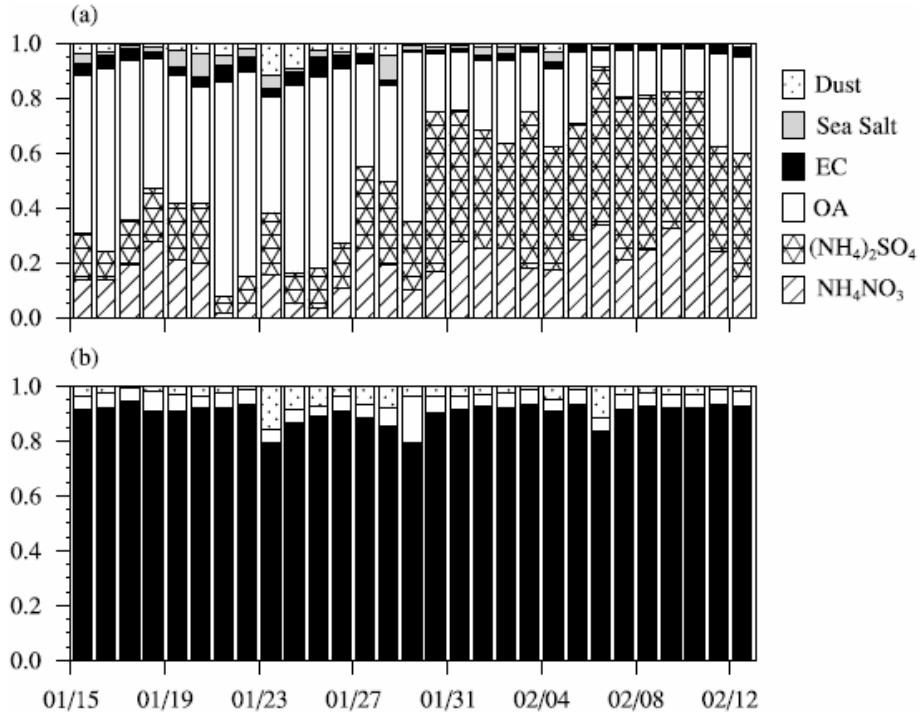

Fig. 7. Time-series of fractional contribution of major aerosol components (i.e. dust, sea salt, elemental carbon (EC), organic aerosol (OA), $(NH_4)_2SO_4$ and NH_4NO_3) to **(a)** the aerosol scattering coefficient and **(b)** the aerosol absorption coefficient, respectively.

ACPD
12, 17151–17185, 2012

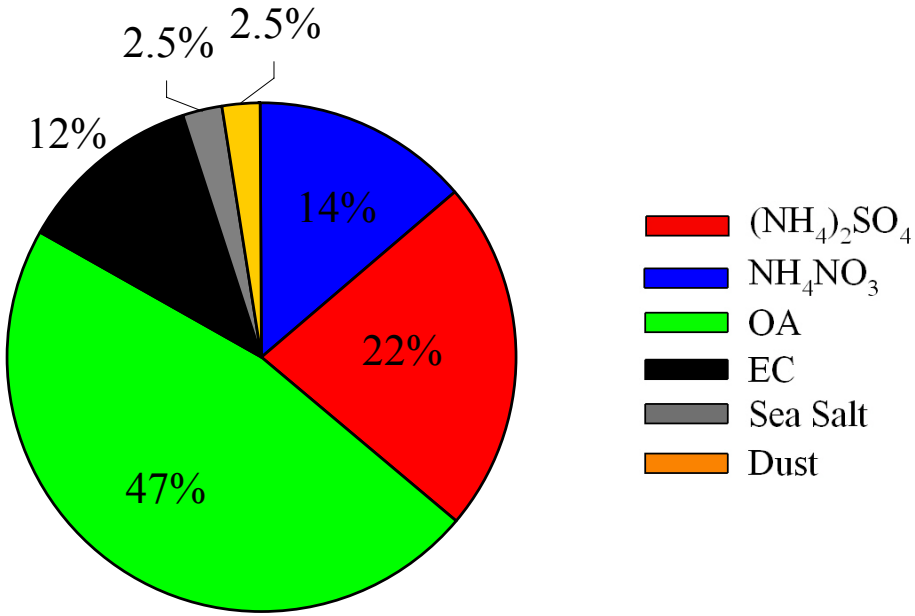

Fig. 8. Fractional contribution of major aerosol components (i.e. SO_4^{2-}, NO_3^-, NH_4^+, organic aerosol (OA), elemental carbon (EC), sea salt and dust) to the total aerosol extinction.

ACPD
12, 17151–17185, 2012